Petroleum Research 11 (2026) 545–555

Contents lists available at ScienceDirect

Petroleum Research

journal homepage: http://www.keaipublishing.com/en/journals/petroleum-research/

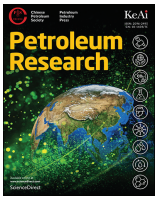

Full Length Article

Experimental investigation of pressure, temperature, and salinity effects on the interfacial tension of H_2/brine/cushion gases: Implications for H_2 geo-storage

Fatemeh Daraii [a], Payam Moradi [a,*], Seyed Ali Bahreini [a], Sina Anvari [b]

[a] Department of Petroleum Engineering, Abadan Faculty of Petroleum Engineering, Petroleum University of Technology (PUT), Abadan, Iran
[b] School of Mining Engineering, College of Engineering, University of Tehran, Tehran, Iran

ARTICLE INFO

Article history:
Received 14 May 2025
Received in revised form
19 November 2025
Accepted 21 November 2025
Available online 25 November 2025

Keywords:
Underground hydrogen storage
Cushion gas
Interfacial tension
High-pressure measurements

ABSTRACT

Underground hydrogen storage (UHS) in saline aquifers is a promising solution for large-scale, long-duration energy storage in a low-carbon energy system. Cushion gases, such as N_2, CO_2, and CH_4, are commonly used to regulate reservoir pressure and enhance storage efficiency. However, despite recent advancements in understanding the interfacial tension (IFT) behavior of H_2–gas mixtures in contact with brine under reservoir conditions, key gaps persist in systematic data for H_2–cushion gas mixtures (e.g., with N_2, CO_2, and CH_4) across specific thermophysical ranges, despite its influence on capillary sealing, gas mobility, and recovery. This study presents systematic experimental measurements of IFT and density for H_2–N_2, H_2–CO_2, and H_2–CH_4 gas mixtures (70:30 mol%) with both distilled water and brine (30,000 ppm NaCl) at different temperatures (25, 50, and 70 °C) and pressures (1, 5, and 10 MPa). The IFT was measured using a high-pressure, high-temperature drop tensiometer, and density was obtained via an Anton Paar DMA 4500 densitometer. Results show a consistent decrease in IFT with rising temperature and pressure across all systems. Notably, the H_2–CH_4 mixture exhibited an IFT of 69.4 mN/m in distilled water at 25 °C and 1 MPa, decreasing to 57.3 mN/m at 70 °C; in contrast, the same mixture in 30,000 ppm brine showed a larger reduction from 61.3 mN/m to 47.8 mN/m under identical conditions, highlighting the amplifying effect of salinity on IFT decline. Among the gas mixtures, CH_4 yielded the approximately lowest overall IFT values, favoring injectivity, whereas N_2 maintained the highest IFT, supporting enhanced capillary retention. These findings address a critical data gap for realistic cushion gas performance and provide foundational insight for modeling UHS in saline aquifers.

1. Introduction

In recent decades, global energy consumption has surged in response to rapid population growth, prompting the development of cleaner and more sustainable energy technologies to combat climate change (Akbari et al., 2025; Ali et al., 2022; Burke and Stephens, 2018; Dawood et al., 2020). Projections suggest that renewable energy sources could contribute 25%–35% of the world's energy needs by 2040 (Gernaat et al., 2021). Hydrogen production and subsurface storage have gained attention as a viable pathway to address rising energy needs, providing a cleaner and more sustainable option compared to traditional fossil fuels (Al-Yaseri and Jha, 2021; Anaya et al., 2023; Tarkowski and Uliasz-Misiak, 2022). Due to its versatility and lower environmental footprint, hydrogen is viewed as a key driver in the shift toward a low-carbon future. It can be generated through various processes, including the conversion of renewable energy (Bechara et al., 2022; Mansir, 2024; Nemmour et al., 2023). To ensure long-term viability, hydrogen must be integrated into existing energy infrastructures, with geo-storage in subsurface formations gaining attention for its practical benefits and scalability (Amirthan and Perera, 2022; Taiwo et al., 2024). As the push for renewable energy intensifies, the successful implementation of H_2 geo-storage will require a thorough understanding of the geological, chemical, and

* Corresponding author.
E-mail addresses: Fateme.daraii.1313@gmail.com (F. Daraii), pmoradi704@gmail.com (P. Moradi), Alibahreini@ait.put.ac.ir (S.A. Bahreini), Sina.anvari@ut.ac.ir (S. Anvari).

Peer review under the responsibility of Editorial Office of Petroleum Research.

https://doi.org/10.1016/j.ptlrs.2025.11.004

mechanical interactions involved (Aftab et al., 2022; Kumar et al., 2023).

Subsurface formations like depleted hydrocarbon reservoirs, deep saline aquifers, and shale layers are considered promising candidates for large-scale underground hydrogen storage (UHS) due to their substantial capacity and geological integrity. Within these porous media, injected hydrogen displaces the existing fluids, typically water or residual hydrocarbons and accumulates beneath impermeable cap rocks, driven by hydrogen's relatively low density (Ebrahimi et al., 2025; Safari et al., 2023; Zeng et al., 2023). The UHS is generally aligned with the operational principles of underground gas storage (UGS) (Oldenburg, 2003). In real-world scenarios, maintaining adequate pressure within the storage formation during hydrogen withdrawal typically necessitates the injection of a cushion gas, such as CO_2, N_2, or CH_4. This cushion gas not only helps sustain reservoir pressure but also minimizes the risk of water encroachment (Kanaani et al., 2022; Muhammed et al., 2023a; Rasool and Hashmi, 2025; Zivar et al., 2021), as illustrated in Fig. 1. In this process, cushion gases are initially introduced into the subsurface formation to establish the necessary pressure conditions prior to hydrogen injection. As hydrogen is subsequently injected, it interacts with the pre-existing cushion gases, resulting in the development of a transitional mixing zone between the two gas phases (Alanazi et al., 2023; Gbadamosi et al., 2023). Despite the critical role of cushion gases in UHS, the extent of their mixing with injected hydrogen, their interactions with formation fluids, and the influence of subsurface flow dynamics remain insufficiently understood (Gbadamosi et al., 2023). To date, limited research has been conducted on how different cushion gases affect the performance and behavior of hydrogen storage systems in geological formations.

Therefore, the existence of hydrogen with varying proportions of cushion gases under different geological storage conditions can significantly affect hydrogen flow behavior during injection/withdrawal cycles. This interplay warrants detailed investigation to better understand and optimize storage performance. Reliable estimation of hydrogen storage capacity in subsurface formations is inherently complex. One of the key challenges is the potential for gas leakage if the injection pressure exceeds the capillary entry pressure of the caprock, leading to possible migration through sealing layers. As a result, the integrity and effective storage capacity of a geological formation are closely governed by capillary pressure (Iglauer, 2011; Iglauer et al., 2015; Li et al., 2006). This pressure is influenced by interfacial tension, contact angle, and pore throat radius, as defined by the Young–Laplace equation (1):

$$P_c = P_g - P_w = \frac{2\sigma \cos\theta}{r} \quad (1)$$

where P_c is the capillary pressure, P_g is the pressure of the gas phase, P_w is the pressure of water, σ is the interfacial tension between water and gas, θ is the contact angle, and r is the effective radius of the pore.

Thus, equation (1) shows that surface tension (σ) is a critical parameter in the diffusion and control of hydrogen storage capacity in subsurface formations (Al-Khdheeawi et al., 2017; Doan et al., 2024). Moreover, evaluating the interfacial tension of hydrogen in contact with subsurface fluids is essential for understanding its fluid dynamics under reservoir conditions. This information plays a critical role in optimizing gas storage efficiency and in designing effective injection/withdrawal strategies (Gbadamosi et al., 2023).

Existing literature reveals that only a limited number of studies have examined the surface tension of hydrogen in contact with pure water or brine. Moreover, experimental data on hydrogen's interfacial behavior in the presence of cushion gases under varying conditions of temperature, pressure, and salinity remain scarce (Chow et al., 2018; Hosseini et al., 2022; Kvamme et al., 2007; Massoudi and King Jr, 1974; Yang et al., 2023). Table 1 provides a comprehensive overview of prior investigations into the IFT between H_2 and aqueous systems under varying thermophysical conditions and cushion gas compositions. The majority of these studies have concentrated on binary systems involving H_2 and either pure water or brine, exploring temperature ranges from 275.15 to 423 K and pressures up to 70 MPa through both experimental and simulation approaches (Kvamme et al., 2007; Massoudi and King Jr, 1974). While these studies have significantly advanced our understanding of H_2–brine interactions, there remains a notable gap in the literature concerning the behavior of H_2 in conjunction with other gases commonly used as cushion gases, such as N_2, CO_2, and CH_4. This gap is particularly evident under conditions that closely mimic those found in subsurface geological formations, where temperature, pressure, and salinity can vary widely. However, until now, there is limited published data exploring how temperature, pressure, and salinity IFT in systems involving hydrogen with cushion gases (CO_2, N_2, and CH_4) in brine. Existing studies on H_2–CH_4–H_2O and H_2–CO_2–H_2O systems have shown that increasing the ratio of cushion gas tends to reduce interfacial tension compared to the binary H_2/H_2O system. This reduction could potentially enhance hydrogen mobility, raising concerns about diffusion through the caprock and increased leakage risks, particularly in the context of hydrogen storage within saline aquifers (Alshammari et al., 2024; Chang et al., 2024b). Alanazi et al. (2023) investigated the interfacial tension of hydrogen in the H_2–CH_4/brine system at pressures of 0.1–1600 psi and temperatures of 323 K. Their results showed that the interfacial tension of H_2–CH_4/brine changed by 53.22 mN/m and 51.17 mN/m with increasing pressure from 0.1 psi to 1600 psi, respectively (Alanazi et al., 2023). Mirchi et al. (2022) investigated IFTs of brine/hydrogen-methane mixtures. Their results showed that the IFT values of H_2–CH_4 mixture/brine diminished with increasing temperature and decreasing hydrogen fraction (Mirchi et al., 2022). Also, Muhammed et al. (2023a) investigated the feasibility of using CH_4 as a cushion gas alongside CO_2 and N_2 for large-scale H_2 storage in depleted natural gas reservoirs, they performed extensive contact angle and surface tension measurements across varying pressures, temperatures, salinities, and gas-mixture compositions to evaluate rock/brine/gas interactions,

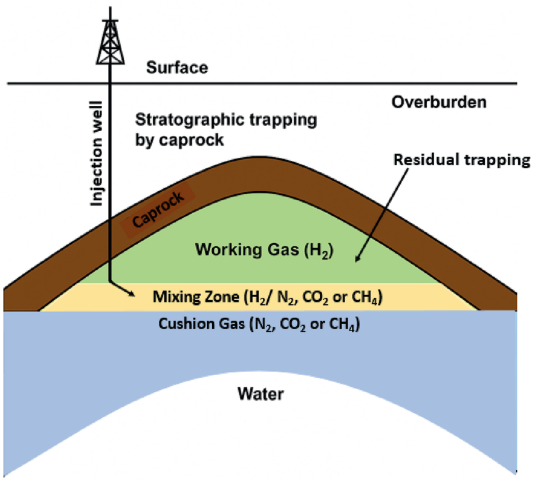

Fig. 1. Schematic of underground hydrogen storage in aquifers and the interaction between hydrogen and cushion gases (CO_2, N_2, and CH_4) (Alanazi et al., 2023).

Table 1
Summary of previous IFT studies between gas mixtures with brine/distilled water in the presence of hydrogen.

Authors	Method	System	Temperature (°k)	Pressure (MPa)
Doan et al. (2024)	Simulation	H_2/CH_4/distilled water	300	1–70
Alanazi et al. (2023)	Experiment	H_2/CH_4/brine	323	0–11
Mirchi et al. (2022)	Experiment	H_2/CH_4/brine	295, 313	6.9
Isfehani et al. (2023)	Experiment	H_2/CO_2/distilled water	323	3–20
Chow et al. (2018)	Experiment	H_2/CO_2/distilled water	298–448	0.5–45
Naeiji et al. (2020)	Simulation	Distilled water/CH_4	275–323	1.4–10
Chow et al. (2016)	Experiment	N_2/CO_2/distilled water	298–448	2–40
Yan et al. (2001)	Experiment	N_2/CO_2/distilled water	298–373	1–30
Silvestri et al. (2019)	Simulation	CO_2/distilled water	308–323	1–50
Kvamme et al. (2007)	Experiment	CO_2/distilled water	278–335	0.1–20
Georgiadis et al. (2010)	Experiment	CO_2/distilled water	298–374	1–60
Doan et al. (2023)	Simulation	H_2/distilled water	298–323	1–70
Shang et al. (2025)	Simulation	H_2/distilled water	298–523	1–160
Massoudi and King Jr (1974)	Experiment	H_2/distilled water	298	7.6
Chow et al. (2018)	Experiment	H_2/distilled water	298–448	0.5–45
Hosseini et al. (2022)	Experiment	H_2/brine	298–423	1–35
Chang et al. (2024a)	Simulation	H_2/CO_2/distilled water H_2/N_2/distilled water H_2/CH_4/distilled water	300–343	1–70
Muhammed et al. (2023b)	Experiment	$H_2/N_2/CO_2/CH_4$/brine	303–343	3–20

their results showed stable wettability across mixtures, surface tension decreasing with temperature and CH_4 fraction, and identified 50–60% H_2 with 30–40% CH_4 as the optimal gas blends for storage applications. In another study, (Muhammed et al., 2023b), examined the effect of using N_2 as a cushion gas (with constant CH_4 and CO_2 proportions) for H_2 storage in depleted natural gas reservoirs, their findings indicated that surface tension decreased with increasing pressure, temperature, and N_2 fraction, identifying mixtures containing 40–60% H_2 and 30–50% N_2 as optimal for storage.

Unlike previous studies that predominantly examined binary H_2–water or H_2–brine systems, or multicomponent mixtures in depleted gas reservoirs, this work specifically investigates the interfacial properties of binary H_2–gas mixtures (H_2–N_2, H_2–CO_2, and H_2–CH_4) in both distilled water and salinity brine (30,000 ppm NaCl). While earlier studies (e.g., Muhammed et al. (2023a)) reported contact angle and surface tension data for multicomponent H_2–CH_4–CO_2–N_2 mixtures in reservoir rocks (Muhammed et al., 2023a), systematic interfacial tension (IFT) and density measurements for binary H_2–gas systems under varying temperature, pressure, and salinity have not been experimentally reported. Here, we extend the analysis by simultaneously measuring IFT and density across a wide range of reservoir-relevant conditions. This approach enables a more accurate application of the Young–Laplace framework and provides the first direct experimental evidence that salinity amplifies IFT reduction in H_2–gas systems. These insights fill a critical gap in the literature by offering reference data for cushion gas selection and capillary-based storage modeling in underground hydrogen storage. Thus, this study provides experimental IFT data for H_2–N_2, H_2–CO_2, and H_2–CH_4 systems under controlled thermophysical conditions, contributing to a more comprehensive understanding of gas–brine interactions essential for predicting containment, optimizing storage design, and ensuring the long-term stability of UHS in saline aquifers.

2. Materials and methods

2.1. Materials

In this study, sodium chloride (NaCl) with a purity of 99.5%, supplied by Merck, was used to prepare the brine solutions. Nitrogen, carbon dioxide, and methane gases, each with a purity greater than 99.99%, were used in the experiments. H_2 gas with 99.999% purity was obtained from Coregas, Australia. The gases were mixed in molar ratios of 70:30 to create H_2–N_2, H_2–CO_2, and H_2–CH_4 gas mixtures (Doan et al., 2024).

2.2. Interfacial tension measurements

To study how temperature, pressure, and salinity affect the IFT of hydrogen and hydrogen-based gas mixtures in brine, a high-pressure, high-temperature drop tensiometer system was used, as shown in Fig. 2. This setup included two syringe pumps for controlling the injection rate and pressure, an LED light source, stainless steel tubing (316 grade), storage accumulators for gas and liquid phases, a PVT (pressure-volume-temperature) cell, and controllers to regulate temperature and pressure. A fine needle (0.4 mm) was used to create the liquid drop, and IFT was measured using online drop analysis software. Before conducting IFT measurements, the gas mixture was transferred from the mixing cylinder to a syringe pump, which was then used to pressurize the measurement cell. In parallel, the brine solution was loaded into a separate syringe pump and injected at a controlled rate of 0.1 cc/min. IFT tests were conducted at a range of pressures (1–10 MPa) and temperatures (25, 50, and 70 °C). All experiments were managed and recorded using the ADVANCE software developed by Krüss. Measurements were performed using both deionized water and a brine solution with 30,000 ppm NaCl. The IFT (γ) between the gas and liquid phases was calculated using the Young–Laplace equation, which relates fluid interface curvature to surface tension:

$$\gamma_{\text{mixture } gas-brine} = \frac{\Delta\rho g}{(\beta k_{apex})^2} \quad (2)$$

in Equation (2), g represents the gravitational acceleration, $\Delta\rho$ refers to the density difference between the gas mixture and brine, k_{apex} describes the interfacial curvature at the drop's apex, and β is a dimensionless parameter characterizing the drop's shape (Navaid et al., 2023). To ensure the reliability and reproducibility of the IFT measurements for each gas–brine system, droplets of fixed volume were formed at a controlled rate of 0.1 cc/min and measured three times. The standard deviation of the results remained below 0.5%, confirming consistency across trials. For validation purposes, the IFT of water against air was also measured under ambient temperature and pressure conditions, yielding a

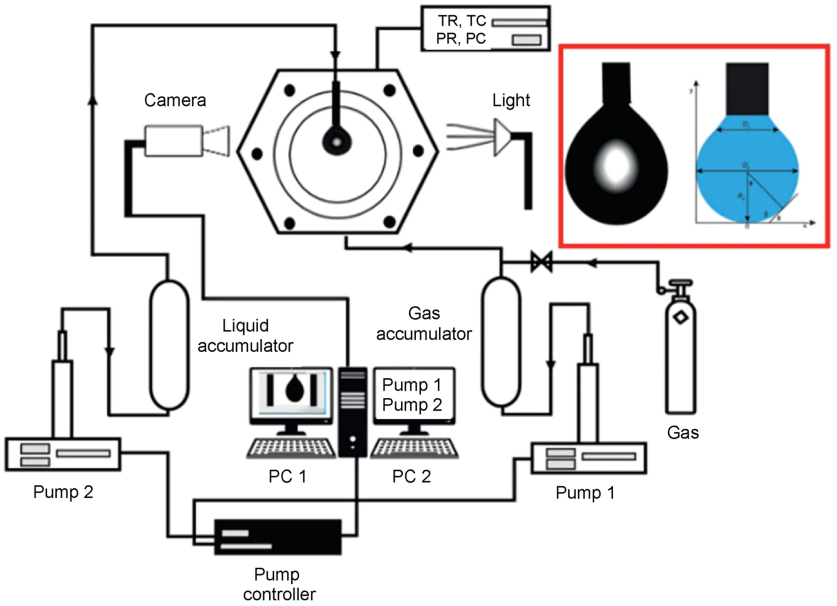

Fig. 2. Experimental setup for measuring IFT under high-temperature and high-pressure conditions.

value of 70.88 mN/m, which closely aligns with previously reported values of 71.6 mN/m and 71.99 mN/m in the literature (Hosseini et al., 2022; Pallas and Harrison, 1990).

2.3. Measurements of density

Measurements of density of solutions were carried out using a high-pressure/high-temperature DMA HP densitometer. To simulate reservoir conditions, measurements were performed at a range of pressures (1, 5, and 10 MPa) and temperatures (25, 50, and 70 °C) for each prepared brine solution. Prior to each test, the measurement tube was carefully rinsed with deionized water to ensure cleanliness, and the brine samples were introduced under controlled temperature and pressure settings to ensure accurate readings.

The density of gas mixtures (H_2–N_2, H_2–CO_2, and H_2–CH_4 at 70-30 vol%) was calculated using the van der Waals equation of state (vdW EOS), which accounts for non-ideal gas behavior by incorporating intermolecular attractions (parameter a) and finite molecular volume (parameter b) (Cheng et al., 2019; Owuna et al., 2024):

$$\left(P+\frac{a_{mix}}{V_m^2}\right)(V_m-b_{mix})=RT \tag{3}$$

$$a_{mix}=\left(\sum_{i=1}x_i\sqrt{a_i}\right)^2 \tag{4}$$

$$b_{mix}=\sum_{i=1}x_i b_i \tag{5}$$

where P is pressure (atm of pa), V is molar volume (L/mol or m^3/mol), R is universal gas constant (0.08314 L bar/K·mol), T is temperature (°K), a_{mix} van der Waals constant for intermolecular attractions (L^2.atm/mol^2), and b_{mix} is finite volume of gas molecules (L/mol). To determine the density of a gas mixture, the laws of mixing must be considered to calculate the effective parameters a and b. The molar mass of each mixture was calculated as a volume-fraction-weighted average of the pure components. The vdW EOS was adapted for mixture density calculations as shown in Equations (3) and (5), using volume-fraction-weighted mixing rules to obtain effective a and b values and the average molar mass of each mixture. This approach improves upon the ideal gas law by partially correcting for molecular interactions, making it suitable for qualitative trend analysis under moderate pressures (1–10 MPa) and temperatures (25–70 °C). Although the vdW EOS accounts for non-ideal effects via attraction (a) and co-volume (b) parameters, its accuracy for gas mixtures, especially at elevated pressures and for CO_2-rich compositions, is limited compared to modern real-gas models (Manuel et al., 2024; Vestfálová and Šafařík, 2018). Recent work by Mohammad Behnamnia et al. (2025) developed an AI-based framework trained on more than

Table 2
Density of brine solutions at different temperature and pressure.

Fluid	Pressure (MPa)	Density (kg/m^3)		
		T_1 = 25 °C	T_1 = 50 °C	T_1 = 70 °C
Deionized water	1	997 ± 2	989 ± 5	980 ± 2
	5	999 ± 2	989 ± 2	982 ± 4
	10	1000 ± 3	995 ± 2	989 ± 3
30,000 ppm NaCl	1	1021 ± 2	1012 ± 3	1001 ± 3
	5	1038 ± 4	1029 ± 4	1018 ± 5
	10	1045 ± 4	1038 ± 3	1031 ± 2

Table 3
Density of gas mixture (H_2–N_2, H_2–CO_2, and H_2–CH_4 at 70:30 vol%).

Mixture	Pressure (MPa)	Density (kg/m^3)		
		T_1 = 25 °C	T_1 = 50 °C	T_1 = 70 °C
H_2:N_2	1	0.40	0.36	0.34
	5	1.98	1.82	1.71
	10	3.95	3.64	3.43
H_2:CO_2	1	0.59	0.54	0.51
	5	2.95	2.72	2.56
	10	5.90	5.44	5.12
H_2:CH_4	1	0.25	0.23	0.21
	5	1.25	1.15	1.09
	10	2.50	2.30	2.17

Table 4
IFT values of H_2–N_2, H_2–CO_2, and H_2–CH_4 in the presence of distilled water and brine in different conditions of temperature, pressure and salinity.

Fluid	Pressure (MPa)	Temperature (°C)	IFT (mN/m)		
			H_2–N_2	H_2–CO_2	H_2–CH_4
Distilled water	1	20	69.25 ± 3	68.19 ± 2	69.35 ± 3
	5	20	67.28 ± 1	67.47 ± 2	65.38 ± 2
	10	20	64.58 ± 3	61.81 ± 1	62.18 ± 4
	1	50	68.52 ± 2	69.61 ± 2	67.89 ± 3
	5	50	59.91 ± 1	62.35 ± 2	60.74 ± 2
	10	50	57.28 ± 2	59.69 ± 2	58.46 ± 4
	1	70	60.37 ± 2	59.68 ± 3	57.28 ± 1
	5	70	56.49 ± 3	55.82 ± 1	54.18 ± 3
	10	70	51.89 ± 2	53.38 ± 2	52.19 ± 1
30,000 ppm NaCl	1	20	65.28 ± 3	66.71 ± 2	66.38 ± 2
	5	20	60.61 ± 3	58.23 ± 3	59.78 ± 1
	10	20	58.41 ± 1	56.12 ± 2	56.89 ± 2
	1	50	61.28 ± 3	62.31 ± 1	63.51 ± 2
	5	50	54.28 ± 2	52.13 ± 4	50.76 ± 2
	10	50	50.31 ± 3	49.89 ± 3	51.43 ± 1
	1	70	56.86 ± 3	55.74 ± 2	55.24 ± 4
	5	70	48.64 ± 1	49.68 ± 2	49.27 ± 1
	10	70	47.21 ± 3	49.57 ± 4	47.82 ± 2

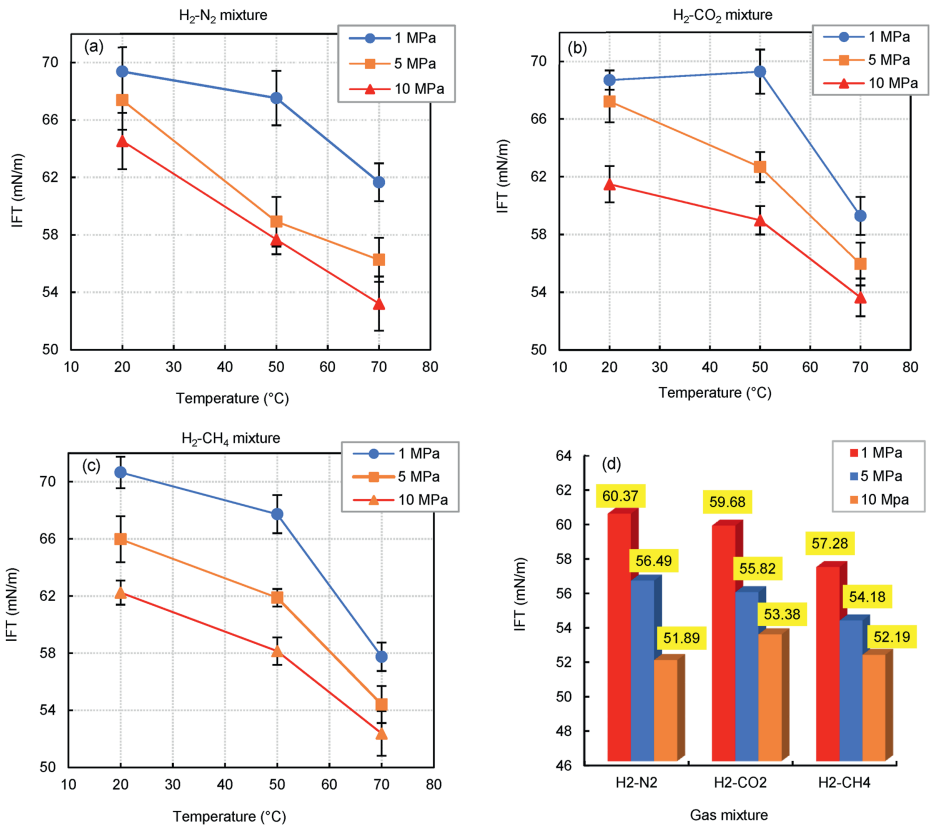

Fig. 3. Pressure and temperature dependence of H_2-gas mixture IFT in distilled water: (a) H_2–N_2 mixture, (b) H_2–CO_2 mixture, (c) H_2–CH_4 mixture, and (d) IFT of gas mixtures at 70 °C.

3300 experimental data points covering H_2 and its mixtures with CH_4, CO_2, and N_2, achieving high accuracy (R^2 = 0.9956, NRMSE = 1.41 %). Incorporating such data-driven or advanced cubic EOS models (e.g., Peng–Robinson equation of state or NIST REFPROP) could further improve the reliability of density estimates (Behnamnia et al., 2025). As this study focuses on comparative trends under controlled conditions, our reported values will serve as a baseline dataset, and future work will validate these results against the reference data provided by Behnamnia et al. (2025).

3. Results and discussion

3.1. Measurements of gas and brine solutions density

The density of brine solutions was determined at different temperatures (25–70 °C) and pressures (1–10 MPa). Density measurements were used in the Young-Laplace equation to calculate IFT. Table 2 shows the density of brine solutions at different temperature and pressure conditions. Each measurement was performed five times and then averaged, and the uncertainty was

expressed as the standard deviation. As shown in Table 2, the density of the solutions varies with both temperature and pressure. An increase in pressure leads to higher solution density, whereas a rise in temperature results in a slight decrease in density.

Table 3 presents the measured densities of the H_2–N_2, H_2–CO_2, and H_2–CH_4 gas mixtures (70:30 vol%) at different pressures and temperatures, calculated using the van der Waals equation of state. The results show that, for all mixtures, density increases markedly with increasing pressure at a constant temperature due to gas phase compression, while it decreases with increasing temperature at a constant pressure because of thermal expansion and reduced gas density. Among the three systems, H_2–CO_2 consistently exhibits the highest densities and H_2–CH_4 the lowest, reflecting the effect of component molar masses and intermolecular interactions on mixture compressibility (Owuna et al., 2024).

3.2. IFT measurements as a function of pressure, temperature, and salinity

Table 4 illustrates the IFT values for the H_2–N_2, H_2–CO_2, and H_2–CH_4 systems in different conditions of temperature of 25, 50, and 70 °C, pressure 1–10 MPa and two salinity levels (distilled water and 30,000 ppm NaCl). As mentioned earlier, each measurement was performed three times, and the average was then calculated. The uncertainty is shown as the standard deviation in Fig. 3 and Table 4. Due to the lack of direct experimental IFT data for H_2–cushion gas–solution systems, available experimental results for H_2–H_2O (Chow et al., 2018; Doan et al., 2023) and CO_2–N_2–H_2O systems (Chow et al., 2016; Yan et al., 2001), as well as simulated data for H_2–CO_2–H_2O, H_2–N_2–H_2O, and H_2–CH_4–H_2O mixtures (Doan et al., 2024), were used as reference points for comparison. According to Fig. 3, all three H_2–cushion gas mixtures in distilled water exhibit a pronounced decrease in IFT with rising temperature and a smaller reduction with increasing pressure. Fig. 4 illustrates the pendant drop profiles of the distilled water in gas mixtures environment at 70 °C. In the H_2–N_2 system (Fig. 3a), IFT falls by approximately 8–9 mN/m as temperature increases from 20 °C to 70 °C, and by about 3 mN/m between 1 bar and 10 bar at a given temperature. The H_2–CO_2 mixture (Fig. 3b) shows a similar overall decline around 8 mN/m over the temperature range and 5 mN/m with pressure, although a slight peak near 50 °C at 1 bar reflects CO_2's solubility behavior. CH_4 produces the highest IFT (Fig. 3c), yet still drops by roughly 12 mN/m with

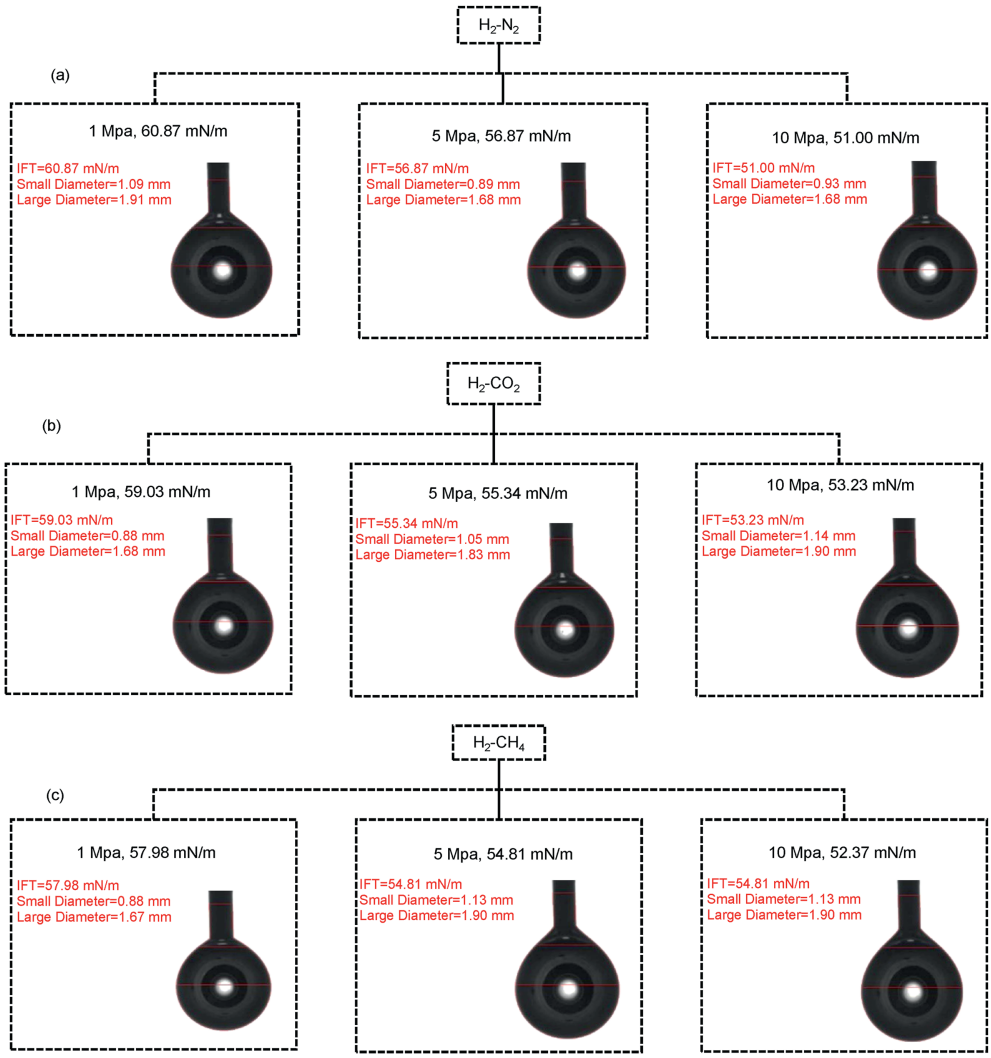

Fig. 4. Pendant drop profiles of distilled water in gas mixtures environment at different pressure (1–10 MPa) and 70 °C: a) H_2–N_2 mixture, b) H_2–CO_2 mixture, and c) H_2–CH_4 mixture.

temperature and 4 mN/m with pressure. These trends align with literature on gas–water interfaces: temperature weakens interfacial cohesion, and higher pressure increases gas density, both of which lower IFT (Al-Yaseri and Jha, 2021; Mirchi et al., 2022; Muhammed et al., 2023b).

According to Fig. 3d, at 70 °C, all three H_2–gas mixtures show a steady decline in IFT as pressure increases from 1 to 10 MPa. For the H_2–N_2 mixture, IFT decreases from about 60 mN/m to 52 mN/m; for H_2–CO_2, from approximately 60 mN/m to 54 mN/m; and for H_2–CH_4, from around 57 mN/m to 52 mN/m. This pressure-induced reduction reflects the classical gas–water interfacial phenomenon, where increasing pressure enhances gas adsorption at the interface, thereby lowering interfacial energy (Massoudi and King Jr, 1974). Unlike typical behavior observed at lower temperatures, at 70 °C the H_2–CO_2 mixture exhibits a slightly higher IFT than the H_2–CH_4 mixture. This is primarily due to the substantial reduction in CO_2 solubility at elevated temperatures, diminishing its ability to lower interfacial tension relative to CH_4 (Alshammari et al., 2024).

CH_4, with its naturally low solubility and weaker temperature dependence (Guo and Rodger, 2013), achieves a lower final IFT despite a smaller relative change. N_2 lies between the two, offering moderate interfacial properties and a balanced IFT profile. For H_2 storage in aquifers, selecting a cushion gas involves optimizing between gas mobility and storage security (Amiri et al., 2024). CH_4, exhibiting lower IFT under these conditions, may facilitate better injectivity and retrieval efficiency, although at the cost of slightly reduced capillary trapping (Amiri et al., 2024). However, N_2 remains an effective intermediate choice, providing a favorable balance between mobility and containment, without the pronounced breakthrough risks associated with highly mobile gases like CO_2 (Lu et al., 2025). The IFTs between gas mixtures and brine at different pressures and temperatures are presented in Fig. 5, whereas the pendant drop profiles of brine in gas mixtures environment at 70 °C are shown in Fig. 6.

In all three gas mixtures in 30,000 ppm NaCl, the IFT remains in a similar numerical range (≈45–63 mN/m) but shows a consistently larger drop with rising temperature and pressure than in distilled water, as shown in the drop profile in Fig. 6. At 20–70 °C and 1–10 MPa, IFT falls by approximately 11–13 mN/m in brine compared to 8–12 mN/m in distilled water, reflecting the additional salinity-induced strengthening of the gas–liquid interface. The salting-out effect raises baseline IFT, but elevated temperature and pressure accelerate ion screening and gas adsorption at the interface, yielding an IFT decline compared to distilled water (Moradi et al., 2024). Among gas mixtures, the rank order of IFT (highest to lowest) remains N_2 > CO_2 > CH_4, but all three see a greater percent reduction in brine (≈20–25 %) than in pure water (≈15–20 %) over the same conditions. For H_2 storage in saline aquifers, this means cushion-gas selection must account not only for absolute IFT but for its enhanced sensitivity to temperature and pressure.

To evaluate the reliability of the measured IFT values, our results were benchmarked against recent literature for similar systems (Fig. 7). For the H_2–N_2 system, the IFT values measured in this study (69.3 → 64.6 mN/m at 25 °C and 1–10 MPa; 68.5 → 57.3 mN/m at 50 °C and 1–10 MPa) closely match the range reported by Doan et al. (2024) (64 → 62 mN/m at 25 °C and 60.3 → 57.3 mN/m at 50 °C) (Doan et al., 2024). Both datasets show a clear decrease in IFT with increasing pressure and temperature, while our additional data in 30,000 ppm NaCl brine confirm a further IFT reduction compared to distilled water, illustrating the salinity-induced interfacial weakening effect. For the H_2–CO_2 system, our values at 50 °C (62.3 and 59.7 mN/m at 5 and 10 MPa in distilled

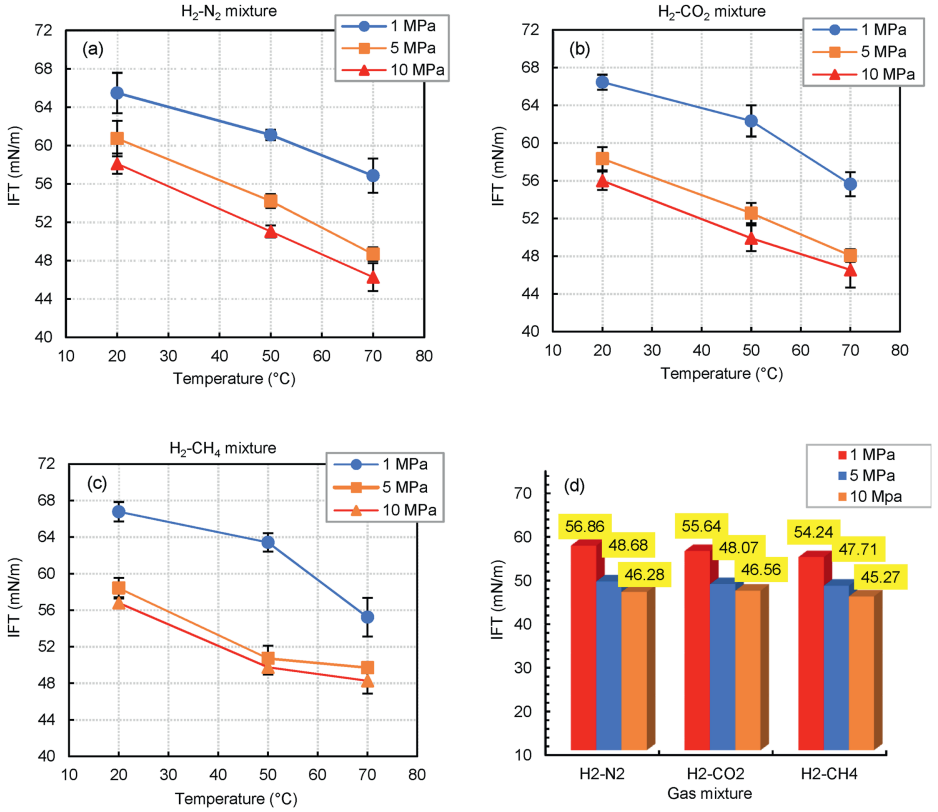

Fig. 5. Pressure and temperature dependence of H_2-gas mixture IFT in brine solution: (a) H_2–N_2 mixture, (b) H_2–CO_2 mixture, (c) H_2–CH_4 mixture, and (d) IFT of gas mixtures at 70 °C.

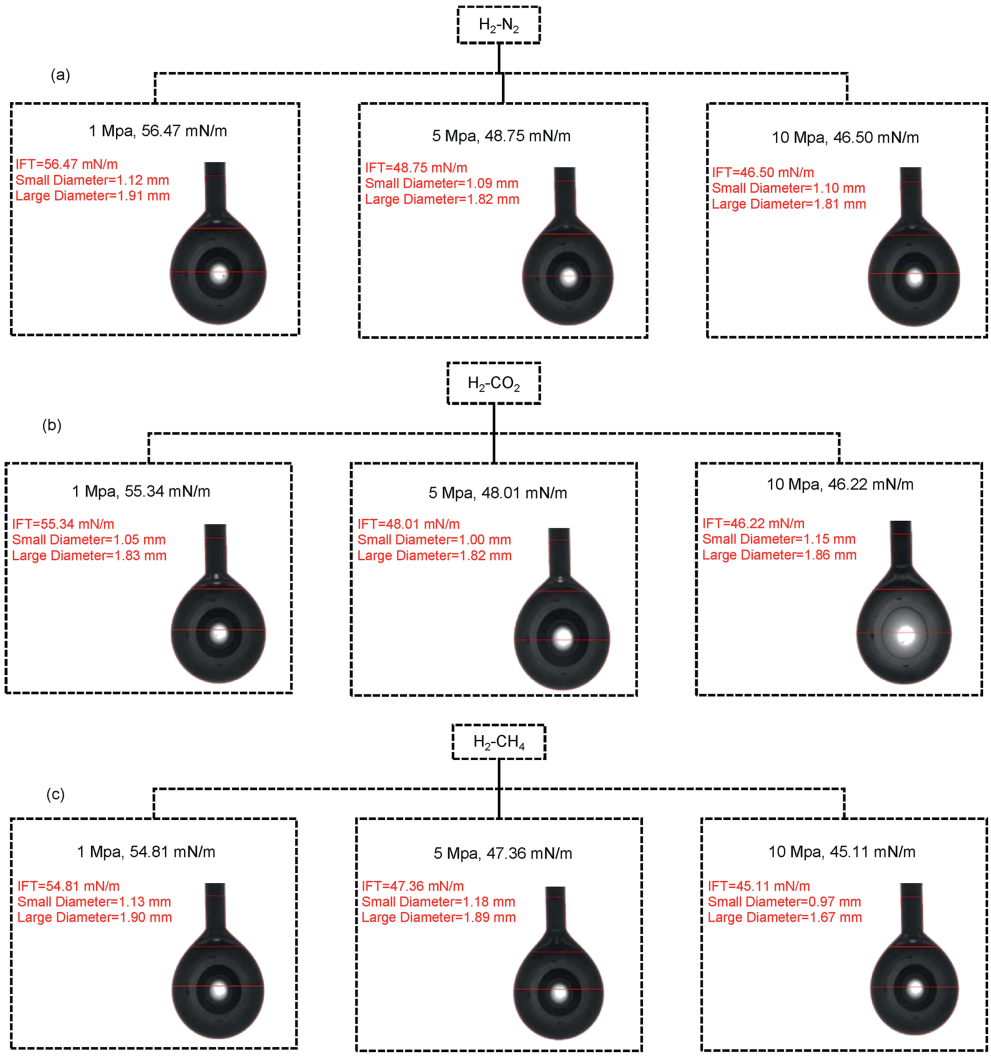

Fig. 6. Pendant drop profiles of brine in gas mixtures environment at different pressure (1–10 MPa) and 70 °C: a) H_2–N_2 mixture, b) H_2–CO_2 mixture, and c) H_2–CH_4 mixture.

water; 53.7 and 49.6 mN/m in 30,000 ppm NaCl brine) are in good agreement with those reported by Isfehani et al. (2023) (62.5 and 57.1 mN/m in distilled water; 64.7–60 mN/m at 1.5 M and 67.3–63.3 mN/m at 3.5 M brine), again showing consistent pressure- and temperature-driven IFT reductions and confirming the salinity-dependent increase reported previously (Isfehani et al., 2023). Similarly, for the H_2–CH_4 system, our data at 50 °C and 30,000 ppm NaCl brine (63.5, 50.8, 51.4 mN/m at 1, 5, 10 MPa) are comparable to the 54.1, 52.5, 50.6 mN/m measured by Alanazi et al. (2023) at 10 % NaCl (Alanazi et al., 2023). Overall, these comparisons demonstrate that our measured IFT values are consistent with the ranges and trends reported in the literature while extending the experimental database to salinity (30,000 ppm NaCl) and a broader pressure–temperature envelope, providing new reference data for modeling gas–brine interfacial behavior under underground hydrogen storage conditions.

The observed IFT trends can be explained by fundamental thermophysical mechanisms at the gas–brine interface. Increasing temperature reduces IFT primarily by weakening the cohesive hydrogen-bond network within the water phase and enhancing the thermal motion of surface molecules, which disrupts interfacial ordering. Increasing pressure compresses the gas phase, raises its density, and promotes molecular adsorption at the interface, thereby lowering the free energy cost of interface formation. Salinity exerts a dual and non-linear effect: at low to moderate concentrations (<1–2 M), dissolved ions screen water–water hydrogen bonding and slightly reduce IFT, but beyond a threshold concentration (typically >2–3 M), strong ion hydration shells and electrostatic ordering in the interfacial region cause “salting-out” of gas molecules and increase the cohesive energy of the interface, thereby raising IFT (Chiquet et al., 2007). This explains why our 30,000 ppm (≈0.5 mol) NaCl results show lower IFT than distilled water, while the 1.5 M and 3.5 M data reported by Isfehani et al. (2023) exhibit higher IFT (Fig. 6c). The consistently lower IFT observed for CH4 mixtures stems from its weak polarity and low aqueous solubility, which limit disruption of water structure and facilitate gas accumulation at the interface. In contrast, N_2 and CO_2 maintain higher IFT due to their greater interfacial free energy, linked to stronger interfacial cohesion, and, in the case of CO_2, partial hydration reactions at the interface (Espinoza and Santamarina, 2010). These mechanisms clarify how temperature, pressure, and salinity jointly govern interfacial cohesion and provide a physical basis for predicting cushion gas behavior during underground hydrogen storage.

Regarded as a clean energy carrier with significant potential to replace fossil fuels, H_2 plays a key role in supporting decarbonization and advancing future energy systems. Among the many technical challenges facing the hydrogen economy, the safe and

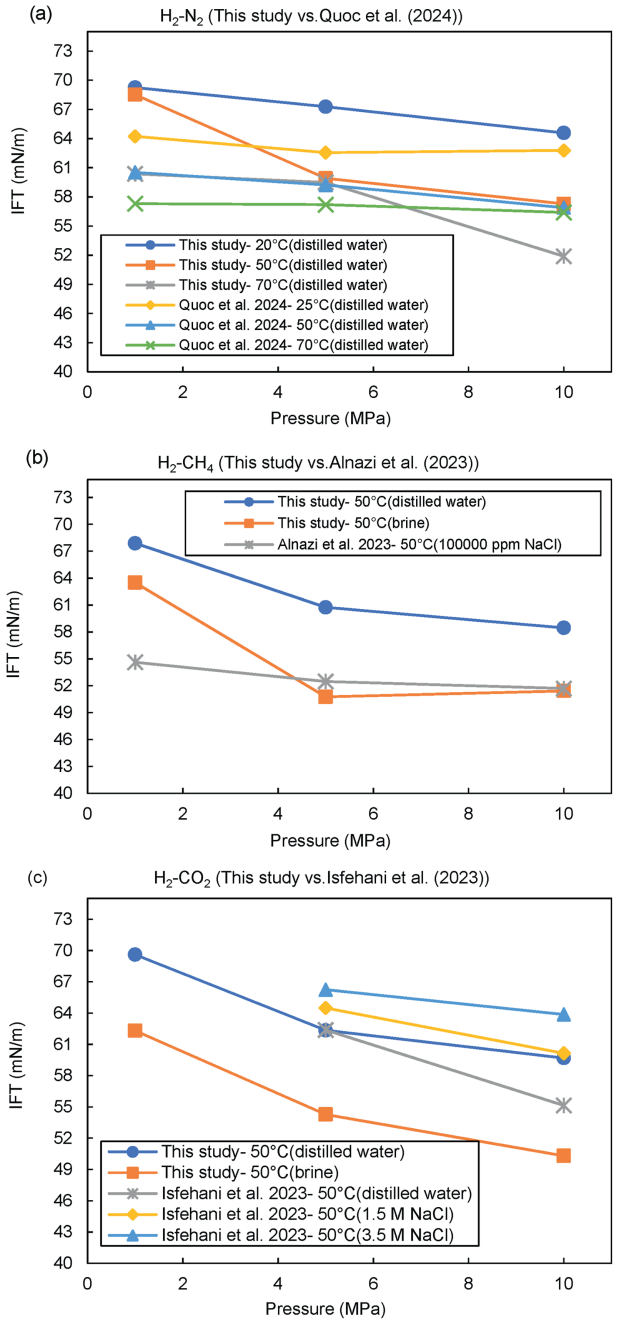

Fig. 7. Comparison of the IFT values from this study with literature data as a function of pressure, temperature, and salinity: (a) H_2–N_2 (this study vs Doan et al., 2024), (b) H_2–CO_2 (this study vs Isfehani et al., 2023), and (c) H_2–CH_4 (this study vs Alanazi et al., 2023).

efficient storage of H_2 remains a major hurdle due to its low density, high diffusivity, and reactive behavior. The IFT trends observed in this study provide critical guidance for selecting cushion gases and designing UHS operations. In capillary-dominated porous media, higher IFT values enhance capillary entry pressure and residual trapping, thereby reducing leakage risk and improving storage security, whereas lower IFT promotes faster gas displacement and higher injectivity but at the expense of containment (Mouallem et al., 2024; Scanziani et al., 2020). The present data show that N_2 consistently exhibits the highest IFT across all tested conditions, indicating its strong potential as a cushion gas for long-term containment-oriented UHS projects, which aligns with previous recommendations of (Behnamnia et al., 2025). CH_4, with the lowest IFT, would favor higher injectivity and operational flexibility but would require stricter seal integrity monitoring to mitigate leakage risk. CO_2 shows intermediate IFT values but is less suitable as a cushion gas because of its known reactivity with reservoir rocks and formation brines, which can induce mineral dissolution, porosity changes, and geochemical alteration (Isfehani et al., 2023). Thus, this study fills that gap by systematically measuring the IFT of H_2–N_2, H_2–CO_2, and H_2–CH_4 mixtures in contact with brine (30,000 ppm NaCl and distilled water) in different temperatures (25, 50, 70 °C) and pressures (1, 5, 10 MPa). The findings provide new insight into how thermophysical and compositional factors influence interfacial properties under reservoir conditions, offering valuable input for reservoir simulation models and the strategic design of future UHS operations.

4. Conclusion

This study systematically investigated the IFT of hydrogen-cushion gas mixtures (H_2–N_2, H_2–CO_2, and H_2–CH_4) in both distilled water and brine (30,000 ppm NaCl) under reservoir-relevant conditions. The key findings are summarized as follows.

- Increasing temperature (20 °C–70 °C) and pressure (1 MPa–10 MPa) consistently reduced IFT across all gas mixtures. For example, in distilled water, the IFT of H_2–CH_4 decreased from 69.35 mN/m (1 MPa, 20 °C) to 52.19 mN/m (10 MPa, 70 °C), demonstrating the strongest sensitivity to thermophysical changes.
- Similar trends were observed in brine, though with higher baseline IFT values. The H_2–N_2 system in brine showed a decline from 65.28 mN/m (1 MPa, 20 °C) to 47.21 mN/m (10 MPa, 70 °C).
- In the brine system, the IFT values of the gas mixtures were lower at all temperature and pressure conditions than in the distilled water system. For instance, H_2–CO_2 in brine at 70 °C and 10 MPa reached 49.57 mN/m, whereas in distilled water, it was 53.38 mN/m under the same conditions.
- CH_4 consistently yielded approximately lowest IFT values, particularly at elevated temperatures and pressures, suggesting enhanced hydrogen mobility but potential leakage risks.
- N_2 and CO_2 showed intermediate behavior, with CO_2 exhibiting unique solubility-driven IFT fluctuations at higher temperatures.

These results emphasise the critical role of cushion gas selection and reservoir conditions in optimizing hydrogen storage efficiency and security. Future work should explore dynamic fluid-rock interactions in porous media to upgrade these findings into practical UHS applications.

CRediT authorship contribution statement

Fatemeh Daraii: Software, Methodology, Investigation. **Payam Moradi:** Writing – review & editing, Writing – original draft, Visualization, Methodology, Investigation, Formal analysis, Conceptualization. **Seyed Ali Bahreini:** Writing – review & editing, Visualization, Validation, Software, Formal analysis. **Sina Anvari:** Writing – review & editing, Software, Data curation.

Declaration of competing interest

Here we confirm that there is no conflict of interest.

Acknowledgements

The authors gratefully acknowledge the Oil and Gas Research Institute of Petroleum University of Technology, Abadan, Iran, for this experimental study.

References

Aftab, A., Hassanpouryouzband, A., Xie, Q., Machuca, L.L., Sarmadivaleh, M., 2022. Toward a fundamental understanding of geological hydrogen storage. Ind. Eng. Chem. Res. 61, 3233–3253.

Akbari, A., Sarvi, H., Maleki, M., Bahreyni, S., Azimi, R., Radpour, A., 2025. Characteristics, emissions, capture, storage, and utilization of carbon dioxide: a comprehensive review of challenges and technologies for greenhouse gas mitigation. Petrol. Res. https://doi.org/10.1016/j.ptlrs.2025.07.001.

Al-Khdheeawi, E.A., Vialle, S., Barifcani, A., Sarmadivaleh, M., Iglauer, S., 2017. Impact of reservoir wettability and heterogeneity on CO2-plume migration and trapping capacity. Int. J. Greenh. Gas Control 58, 142–158.

Al-Yaseri, A., Jha, N.K., 2021. On hydrogen wettability of basaltic rock. J. Petrol. Sci. Eng. 200, 108387.

Alanazi, A., Yekeen, N., Ali, M., Ali, M., Abu-Mahfouz, I.S., Keshavarz, A., Iglauer, S., Hoteit, H., 2023. Influence of organics and gas mixing on hydrogen/brine and methane/brine wettability using Jordanian oil shale rocks: implications for hydrogen geological storage. J. Energy Storage 62, 106865.

Ali, M., Jha, N.K., Pal, N., Keshavarz, A., Hoteit, H., Sarmadivaleh, M., 2022. Recent advances in carbon dioxide geological storage, experimental procedures, influencing parameters, and future outlook. Earth Sci. Rev. 225, 103895.

Alshammari, S., Abdel-Azeim, S., Al-Yaseri, A., Qasim, A., 2024. The influence of CH4 and CO2 on the interfacial tension of H2–brine, water–H2–rock wettability, and their implications on geological hydrogen storage. Energy Fuel. 38, 15834–15847.

Amiri, I.I., Zivar, D., Ayatollahi, S., Mahani, H., 2024. The effect of gas solubility on the selection of cushion gas for underground hydrogen storage in aquifers. J. Energy Storage 80, 110264.

Amirthan, T., Perera, M., 2022. The role of storage systems in hydrogen economy: a review. J. Nat. Gas Sci. Eng. 108, 104843.

Anaya, K., Oni, A.O., Kumar, A., 2023. Investigating the techno-economic and environmental performance of chemical looping technology for hydrogen production. Sustain. Energy Technol. Assessments 56, 103008.

Bechara, E., Gamadi, T., Hussain, A., Emadibaladehi, H., 2022. Effect of hydrogen exposure on shale reservoir properties and evaluation of hydrogen storage possibility in depleted unconventional formations. In: Unconventional Resources Technology Conference, 20–22 June 2022. Unconventional Resources Technology Conference (URTeC), pp. 1734–1748.

Behnamnia, M., Sarvi, H., Monfared, A.D., 2025. Leveraging AI for accurate prediction of hydrogen density (in pure/mixed form): implications for hydrogen energy transition processes. Renew. Energy, 123447.

Burke, M.J., Stephens, J.C., 2018. Political power and renewable energy futures: a critical review. Energy Res. Social Sci. 35, 78–93.

Chang, Q., Dempsey, D., Huang, L., 2024a. Simulations of interfacial tension for H2/H2S/Water and CH4/H2S/Water systems at the temperature of 298 K and pressure up to 30 MPa. In: SPE Asia Pacific Oil and Gas Conference and Exhibition. SPE, D011S006R002.

Chang, Q., Dempsey, D., Zhang, L., Zhao, Y., Huang, L., 2024b. Molecular dynamics insights into gas-water interfacial tension: optimizing hydrogen storage in subsurface conditions. Int. J. Hydrogen Energy 64, 896–905.

Cheng, S., Shang, F., Ma, W., Jin, H., Sakoda, N., Zhang, X., Guo, L., 2019. Density data of two (H2+ CO2) mixtures and a (H2+ CO2+ CH4) mixture by a modified burnett method at temperature 673 K and pressures up to 25 MPa. J. Chem. Eng. Data 64, 1693–1704.

Chiquet, P., Broseta, D., Thibeau, S., 2007. Wettability alteration of caprock minerals by carbon dioxide. Geofluids 7, 112–122.

Chow, Y.F., Maitland, G.C., Trusler, J.M., 2016. Interfacial tensions of the (CO2+ N2+ H2O) system at temperatures of (298 to 448) K and pressures up to 40 MPa. J. Chem. Therm. 93, 392–403.

Chow, Y.F., Maitland, G.C., Trusler, J.M., 2018. Interfacial tensions of (H2O+ H2) and (H2O+ CO2+ H2) systems at temperatures of (298–448) K and pressures up to 45 MPa. Fluid Phase Equilib. 475, 37–44.

Dawood, F., Anda, M., Shafiullah, G., 2020. Hydrogen production for energy: an overview. Int. J. Hydrogen Energy 45, 3847–3869.

Doan, Q.T., Keshavarz, A., Miranda, C.R., Behrenbruch, P., Iglauer, S., 2023. Molecular dynamics simulation of interfacial tension of the CO2-CH4-water and H2-CH4-water systems at the temperature of 300 K and 323 K and pressure up to 70 MPa. J. Energy Storage 66, 107470.

Doan, Q.T., Keshavarz, A., Miranda, C.R., Behrenbruch, P., Iglauer, S., 2024. A prediction of interfacial tension by using molecular dynamics simulation: a study on effects of cushion gas (CO2, N2 and CH4) for underground hydrogen storage. Int. J. Hydrogen Energy 50, 1607–1615.

Ebrahimi, A., Ghasemi, K., Akbari, A., Kazemzadeh, Y., Azin, R., 2025. Hydrogen energy system and underground hydrogen storage in depleted reservoirs. Petrol. Res.10(3), 501-528.

Espinoza, D.N., Santamarina, J.C., 2010. Water-CO2-mineral systems: interfacial tension, contact angle, and diffusion—Implications to CO2 geological storage. Water Resour. Res. 46.

Gbadamosi, A.O., Muhammed, N.S., Patil, S., Al Shehri, D., Haq, B., Epelle, E.I., Mahmoud, M., Kamal, M.S., 2023. Underground hydrogen storage: a critical assessment of fluid-fluid and fluid-rock interactions. J. Energy Storage 72, 108473.

Georgiadis, A., Maitland, G., Trusler, J.M., Bismarck, A., 2010. Interfacial tension measurements of the (H2O+ CO2) system at elevated pressures and temperatures. J. Chem. Eng. Data 55, 4168–4175.

Gernaat, D.E., de Boer, H.S., Daioglou, V., Yalew, S.G., Müller, C., van Vuuren, D.P., 2021. Climate change impacts on renewable energy supply. Nat. Clim. Change 11, 119–125.

Guo, G.-J., Rodger, P.M., 2013. Solubility of aqueous methane under metastable conditions: implications for gas hydrate nucleation. J. Phys. Chem. B 117, 6498–6504.

Hosseini, M., Fahimpour, J., Ali, M., Keshavarz, A., Iglauer, S., 2022. H2− brine interfacial tension as a function of salinity, temperature, and pressure; implications for hydrogen geo-storage. J. Petrol. Sci. Eng. 213, 110441.

Iglauer, S., 2011. Dissolution Trapping of Carbon Dioxide in Reservoir Formation brine-a Carbon Storage Mechanism. INTECH Open Access Publisher, London, UK.

Iglauer, S., Pentland, C., Busch, A., 2015. CO2 wettability of seal and reservoir rocks and the implications for carbon geo-sequestration. Water Resour. Res. 51, 729–774.

Isfehani, Z.D., Sheidaie, A., Hosseini, M., Fahimpour, J., Iglauer, S., Keshavarz, A., 2023. Interfacial tensions of (brine+ H2+ CO2) systems at gas geo-storage conditions. J. Mol. Liq. 374, 121279.

Kanaani, M., Sedaee, B., Asadian-Pakfar, M., 2022. Role of cushion gas on underground hydrogen storage in depleted oil reservoirs. J. Energy Storage 45, 103783.

Kumar, K.R., Honorio, H., Chandra, D., Lesueur, M., Hajibeygi, H., 2023. Comprehensive review of geomechanics of underground hydrogen storage in depleted reservoirs and salt caverns. J. Energy Storage 73, 108912.

Kvamme, B., Kuznetsova, T., Hebach, A., Oberhof, A., Lunde, E., 2007. Measurements and modelling of interfacial tension for water+ carbon dioxide systems at elevated pressures. Comput. Mater. Sci. 38, 506–513.

Li, Z., Dong, M., Li, S., Huang, S., 2006. CO2 sequestration in depleted oil and gas reservoirs—caprock characterization and storage capacity. Energy Convers. Manag. 47, 1372–1382.

Lu, J., Muhammed, N.S., Okolie, J.A., Epelle, E.I., 2025. A sensitivity study of hydrogen mixing with cushion gases for effective storage in porous media. Sustain. Energy Fuels 9, 1353–1370.

Mansir, I.B., 2024. Thermodynamic investigation of novel hybrid plant with hydrogen as a green energy carrier. Int. J. Hydrogen Energy 51, 1171–1180.

Manuel, N., Major, T., Pedro, S., Barros, A., 2024. Use the thermodynamic state equations to analyze the non-ideality of gas mixtures. Int. J. Therm. 27, 43–50.

Massoudi, R., King, Jr, A., 1974. Effect of pressure on the surface tension of water. Adsorption of low molecular weight gases on water at 25. deg. J. Phys. Chem. 78, 2262–2266.

Mirchi, V., Dejam, M., Alvarado, V., 2022. Interfacial tension and contact angle measurements for hydrogen-methane mixtures/brine/oil-wet rocks at reservoir conditions. Int. J. Hydrogen Energy 47, 34963–34975.

Moradi, P., Simjoo, M., Chahardowli, M., 2024. Experimental insights into the effect of aquifer salinity on interfacial properties of fluorinated surfactants: relevant for underground gas storage. J. Mol. Liq. 414, 126203.

Mouallem, J., Arif, M., Raza, A., Glatz, G., Rahman, M.M., Mahmoud, M., Iglauer, S., 2024. Critical review and meta-analysis of the interfacial tension of CO2-brine and H2-brine systems: implications for CO2 and H2 geo-storage. Fuel 356, 129575.

Muhammed, N.S., Haq, B., Al Shehri, D., 2023a. Role of methane as a cushion gas for hydrogen storage in depleted gas reservoirs. Int. J. Hydrogen Energy 48, 29663–29681.

Muhammed, N.S., Haq, B., Al Shehri, D.A., 2023b. Hydrogen storage in depleted gas reservoirs using nitrogen cushion gas: a contact angle and surface tension study. Int. J. Hydrogen Energy 48, 38782–38807.

Naeiji, P., Woo, T.K., Alavi, S., Ohmura, R., 2020. Molecular dynamics simulations of interfacial properties of the CO2–water and CO2–CH4–water systems. J. Chem. Phys. 153.

Navaid, H.B., Emadi, H., Watson, M., 2023. A comprehensive literature review on the challenges associated with underground hydrogen storage. Int. J. Hydrogen Energy 48, 10603–10635.

Nemmour, A., Inayat, A., Janajreh, I., Ghenai, C., 2023. Green hydrogen-based E-fuels (E-methane, E-methanol, E-ammonia) to support clean energy transition: a literature review. Int. J. Hydrogen Energy 48, 29011–29033.

Oldenburg, C.M., 2003. Carbon dioxide as cushion gas for natural gas storage. Energy Fuel. 17, 240–246.

Owuna, F.J., Chapoy, A., Ahmadi, P., Burgass, R., 2024. Experimental (ρ, P, T) data of H2+ CH4 mixtures at temperatures from 278 to 398 K and pressures up to 56 MPa. Int. J. Hydrogen Energy 68, 979–997.

Pallas, N.R., Harrison, Y., 1990. An automated drop shape apparatus and the surface tension of pure water. Colloids Surf. 43, 169–194.

Rasool, M.H., Hashmi, S.A.M., 2025. Carbon capture and storage: an evidence-based review of its limitations and missed promises. Petrol. Res. https://doi.org/

10.1016/j.ptlrs.2025.09.005.
Safari, A., Zeng, L., Nguele, R., Sugai, Y., Sarmadivaleh, M., 2023. Review on using the depleted gas reservoirs for the underground H2 storage: a case study in Niigata prefecture, Japan. Int. J. Hydrogen Energy 48, 10579–10602.
Scanziani, A., Singh, K., Menke, H., Bijeljic, B., Blunt, M.J., 2020. Dynamics of enhanced gas trapping applied to CO2 storage in the presence of oil using synchrotron X-ray micro tomography. Appl. Energy 259, 114136.
Shang, Z., Yang, Y., Li, J., Zhang, Q., Zhang, L., Sun, H., Zhong, J., Zhang, K., Yao, J., 2025. Molecular dynamics insights into interfacial tension and solubility of hydrogen-cushion gas-water systems for underground hydrogen storage. Geoenergy Sci. Eng., 214215
Silvestri, A., Ataman, E., Budi, A., Stipp, S., Gale, J.D., Raiteri, P., 2019. Wetting properties of the CO2–water–calcite system via molecular simulations: shape and size effects. Langmuir 35, 16669–16678.
Taiwo, G.O., Tomomewo, O.S., Oni, B.A., 2024. A comprehensive review of underground hydrogen storage: insight into geological sites (mechanisms), economics, barriers, and future outlook. J. Energy Storage 90, 111844.
Tarkowski, R., Uliasz-Misiak, B., 2022. Towards underground hydrogen storage: a review of barriers. Renew. Sustain. Energy Rev. 162, 112451.
Vestfálová, M., Šafařík, P., 2018. Determination of the applicability limits of the ideal gas model for the calculation of moist air properties. In: EPJ Web of Conferences. EDP Sciences, 02115.
Yan, W., Zhao, G.-Y., Chen, G.-J., Guo, T.-M., 2001. Interfacial tension of (methane+ nitrogen)+ water and (carbon dioxide+ nitrogen)+ water systems. J. Chem. Eng. Data 46, 1544–1548.
Yang, Y., Nair, A.K.N., Zhu, W., Sang, S., Sun, S., 2023. Molecular perspectives of interfacial properties of the hydrogen+ water mixture in contact with silica or kerogen. J. Mol. Liq. 385, 122337.
Zeng, L., Vialle, S., Ennis-King, J., Esteban, L., Sarmadivaleh, M., Sarout, J., Dautriat, J., Giwelli, A., Xie, Q., 2023. Role of geochemical reactions on caprock integrity during underground hydrogen storage. J. Energy Storage 65, 107414.
Zivar, D., Kumar, S., Foroozesh, J., 2021. Underground hydrogen storage: a comprehensive review. Int. J. Hydrogen Energy 46, 23436–23462.